Acta Pharmacologica Sinica

www.nature.com/aps

ARTICLE

Effect of autoinduction and food on the pharmacokinetics of furmonertinib and its active metabolite characterized by a population pharmacokinetic model

Hui-xi Zou[1], Yu-feng Zhang[1], Da-fang Zhong[2], Yong Jiang[3], Fei Liu[3], Qian-yu Zhao[3], Zhong Zuo[1], Yi-fan Zhang[2] and Xiao-yu Yan[1]

Furmonertinib (AST2818) is a novel third-generation irreversible EGFR TKI and recently has been approved in China for the treatment of non-small cell lung cancer (NSCLC) with EGFR-sensitizing and T790M resistance mutations. In the current study, we developed a semi-mechanistic population pharmacokinetic model to characterize the nonstationary pharmacokinetics (PK) of the furmonertinib and its active metabolite AST5902 simultaneously. The PK data of furmonertinib and AST5902 were obtained from 38 NSCLC patients and 16 healthy volunteers receiving 20–240 mg furmonertinib in three clinical trials. A nonlinear mixed-effects modeling approach was used to describe the PK data. The absorption process of furmonertinib was described by a transit compartment model. The disposition of both furmonertinib and AST5902 was described by a two-compartment model. An indirect response model accounted for the autoinduction of furmonertinib metabolism mediated by CYP3A4. The model-based simulation suggested that furmonertinib clearance was increased in one cycle of treatment (orally once daily for 21 days) compared to baseline, ranging from 1.1 to 1.8 fold corresponding to the dose range of 20–240 mg. The concentration of furmonertinib was decreased over time whereas that of AST5902 was increased. Interestingly, the concentration of the total active compounds (furmonertinib and AST5902) appeared to be stable. The food intake, serum alkaline phosphatase and body weight were identified as statistically significant covariates. The mechanism of food effect on PK was investigated, where the food intake might increase the bioavailability of furmonertinib via increasing the splanchnic blood flow. Overall, a population PK model was successfully developed to characterize the nonstationary PK of furmonertinib and AST5902 simultaneously. The concentrations of total active compounds were less affected by the autoinduction of furmonertinib metabolism.

Keywords: furmonertinib; autoinduction; food effect; alkaline phosphatase; body weight; pharmacokinetics; modeling and simulation; NSCLC

Acta Pharmacologica Sinica (2022) 43:1865–1874; https://doi.org/10.1038/s41401-021-00798-y

INTRODUCTION

Non-small cell lung cancer (NSCLC) accounts for ~75%–85% of all types of lung cancer [1, 2]. Epidermal growth factor receptor (EGFR) is one of several somatic mutations in NSCLC [3, 4]. The first- and second-generation EGFR tyrosine kinase inhibitors (TKIs) have been recommended as the first-line therapy for NSCLC patients with EGFR mutation [5–9]. Unfortunately, previous studies have found that patients who have a good initial response may ultimately show resistance to the treatment [10–12]. The most common resistance mechanism is driven by the acquisition of a T790M EGFR TKI resistance mutation (50%) [13, 14], based on which the third-generation EGFR-TKIs were developed to target both EGFR-sensitizing and T790M resistance mutations [15]. Osimertinib is one of the third-generation EGFR-TKIs and has been approved for NSCLC patients who have progressed disease on or after prior EGFR TKI therapy [16].

Furmonertinib (AST2818) is a novel third-generation irreversible EGFR TKI and recently received approval by the National Medical Products Administration (NMPA) of China for the treatment of NSCLC with EGFR-sensitizing and T790M resistance mutations [17–19]. Previous clinical studies demonstrated that furmonertinib was well tolerated and exhibited clinical efficacy in EGFR T790M-positive NSCLC patients, who had progressed following first-generation or second-generation EGFR-TKIs treatment [17, 18]. At present, an ongoing phase III clinical trial of furmonertinib (FLAG, NCT03787992) is conducted in locally advanced or metastatic NSCLC patients to assess the efficacy and safety as the first-line treatment.

Furmonertinib is predominantly metabolized by CYP3A4 to form a pharmacologically active metabolite AST5902, which has a similar antitumor activity to furmonertinib [17–20]. This metabolite has been identified as the major metabolite of furmonertinib and has a comparable exposure to that of furmonertinib in patients treated with multiple oral doses of furmonertinib [18]. Since furmonertinib is a potent CYP3A4 inducer, its administrations may result in the nonstationary PK of furmonertinib and AST5902 in patients [19].

[1]School of Pharmacy, Faculty of Medicine, The Chinese University of Hong Kong, Hong Kong, China; [2]State Key Laboratory of Drug Research, Shanghai Institute of Materia Medica, Chinese Academy of Sciences, Shanghai 201203, China and [3]Shanghai Allist Pharmaceutical Technology Co., Ltd., Shanghai 201203, China
Correspondence: Yi-fan Zhang (yfzhang@simm.ac.cn) or Xiao-yu Yan (xiaoyuyan@cuhk.edu.hk)

Received: 10 June 2021 Revised: 14 October 2021 Accepted: 14 October 2021
Published online: 17 November 2021

This study aimed to develop a semi-mechanistic pharmacokinetic model to characterize the nonstationary PK of furmonertinib and its active metabolite AST5902 simultaneously. The PK data of furmonertinib and AST5902 were obtained from NSCLC patients ($n = 38$) and healthy volunteers ($n = 16$) given 20–240 mg furmonertinib in three clinical trials [18, 20]. An indirect response model was used to describe the autoinduction of furmonertinib metabolism. The impact of food effect on the PK of furmonertinib and the AST5902 is complex [20], where the exposure of furmonertinib increased within food intake whereas that of active metabolite AST5902 decreased. Thus, the influences of food intake on the PK of furmonertinib and its active metabolite AST5902 were investigated. Also, the effects of the demographic characteristics on drug exposure were assessed and quantified.

MATERIALS AND METHODS

All studies were conducted in China following the Good Clinical Practice guidelines and the principles of the Declaration of Helsinki. The protocol, amendments, and informed consent were approved by the independent ethics committee at each participating site [18, 20]. Written informed consent was obtained from all subjects before screening in each study.

Study population

Study 001 (dose-escalation, NCT02973763) and Study 002 (dose-expansion, NCT03127449) were open-label, single-arm and multicenter studies as described by us before [18]. Briefly, Study 001 was a phase I study in NSCLC patients with EGFR T790M mutation. These patients had disease progression on previous therapy with first-generation or second-generation EGFR-TKIs treatment. Study 002 was a phase I/II study in a similar patient population as Study 001. Study 004 (food-effect study, NCT03926182) was an open-label, cross-over, two-period, randomized and sequential study to investigate the food effect on the PK of furmonertinib [20]. In Study 004, participants included healthy men with 18–55 years of age who had a body mass index (BMI) between 19 and 26 kg/m^2 and weight between 50 and 80 kg.

Study design

Study 001 was designed to evaluate the safety and tolerability of furmonertinib in NSCLC patients. The following doses were assessed in five cohorts: 20, 40, 80, 160 and 240 mg [18]. Each cohort consisted of a single-dose period (7 d) followed by a multiple-dose period (once daily, 21 d per cycle). To obtain the full PK profile, blood samples were collected at predose, 0.5, 1, 1.5, 2, 3, 4, 6, 8, 10, 12, 24, 48, and 72 h after the first or the multiple-dose treatment (on cycle 2 day 1, steady state). Additional predose blood samples were collected on cycle 1 day 1, 8, and 15. Based on the results of Study 001, three doses (80, 160, and 240 mg) were selected in Study 002 for further evaluation [18]. In Study 002, each dose group included 8 patients receiving oral administration of furmonertinib (once daily, 21 d per cycle). Same as Study 001, blood samples after the first and the multiple-dose treatment (on cycle 2 day 1, steady state) were collected to obtain the full PK profile at predose, 0.5, 1, 1.5, 2, 3, 4, 6, 8, 10, 12, and 24 h. Additional predose blood samples were collected as well. Patients in Study 001 and Study 002 all received the furmonertinib administration under fasting conditions.

Study 004 is a crossover study to assess the food effect on the PK of furmonertinib in 16 healthy male subjects [20]. All subjects received a single oral dose of 80 mg furmonertinib after an overnight fast of at least 10 h, or immediately after ingestion of a high-fat, high-calorie breakfast. These treatments were separated by a period of 22 days. Blood samples for PK analysis were collected at predose, 0.5, 1, 2, 3, 4, 6, 8, 10, 12, 24, 48, 72, 120, 168, 216, 336, and 504 h after dosing.

All the collected plasma samples were subjected to analyses of furmonertinib and AST5902 by liquid chromatography-tandem mass spectrometry (LC/MS/MS) to characterize their PK profiles as we described before [21]. The lower limits of quantification (LLOQ) of furmonertinib and AST5902 were 0.20 and 0.050 ng/mL, respectively.

Model development and evaluation

Structural model building. The structural PK model for furmonertinib and its active metabolite AST5902 after oral administration is presented in Fig. 1. The absorption of furmonertinib after oral administration was described by a transit compartment model. As demonstrated in Fig. 1, the drug entered from the depot compartment and into the central compartment via two transit compartments. The absorption and the transfer rate were quantified by k_a. The disposition of furmonertinib was described by a two-compartment model. Due to the lack of PK data after intravenous administration to estimate the bioavailability of furmonertinib (F), the model of furmonertinib was parameterized in terms of apparent clearance (CL/F), apparent volume of distribution of the central (V_c/F) and peripheral (V_p/F) compartment, and apparent intercompartment clearance (Q/F).

To describe the PK of AST5902, furmonertinib was assumed to be eliminated through the central compartment, in which a fraction (Fm) of furmonertinib was metabolized to AST5902. Due to

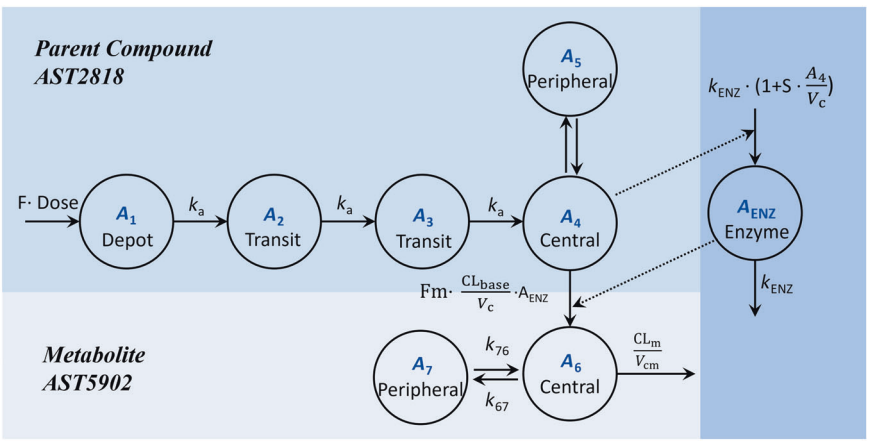

Fig. 1 Schematic of the PK model of furmonertinib (AST2818) and AST5902. The PK of the parent compound furmonertinib was described by a two-compartment model with a transit compartment absorption chain. The disposition of the active metabolite AST5902 was described by a two-compartment model with first-order elimination. An indirect response model and an enzyme compartment are used to describe the autoinduction on furmonertinib metabolism.

the lack of intravenous PK data of furmonertinib and AST5902, it was not possible to simultaneously estimate the actual value of the fraction of conversion to AST5902 and the volume of distribution of the AST5902 [22]. Thus, the apparent clearance [$Cl_m/(F \cdot Fm)$] and apparent volume of distribution of the central compartment [$V_{cm}/(F \cdot Fm)$] of AST5902 were estimated. AST5902 in the central compartments can distribute to the peripheral compartment via distribution rate constants k_{67} and k_{76}. The differential equations for the PK model (Fig. 1) are expressed as follows:

$$\frac{dA_1}{dt} = -k_a \cdot A_1 \quad (1)$$

$$\frac{dA_2}{dt} = k_a \cdot A_1 - K_a \cdot A_2 \quad (2)$$

$$\frac{dA_3}{dt} = K_a \cdot A_2 - K_a \cdot A_3 \quad (3)$$

$$\frac{dA_4}{dt} = K_a \cdot A_3 - \frac{CL}{V_c} \cdot A_4 - \frac{Q}{V_c} \cdot A_4 + \frac{Q}{V_p} \cdot A_5 \quad (4)$$

$$\frac{dA_5}{dt} = \frac{Q}{V_c} \cdot A_4 - \frac{Q}{V_p} \cdot A_5 \quad (5)$$

$$\frac{dA_6}{dt} = \frac{CL}{V_c} \cdot A_4 \cdot Fm - \frac{Cl_m}{V_{cm}} \cdot A_6 - K_{67} \cdot A_6 + K_{76} \cdot A_7 \quad (6)$$

$$\frac{dA_7}{dt} = K_{67} \cdot A_6 - K_{76} \cdot A_7 \quad (7)$$

The initial values of A_1 was set to (Dose · F), and the initial values of A_2 to A_7 were all set to zero. A_1, A_4, and A_5 represent the amounts of furmonertinib in the depot, central, and peripheral compartment, respectively; A_2 and A_3 represent the furmonertinib amounts in the absorption transit compartments; A_6 and A_7 represent the amounts of AST5902 in the central and peripheral compartments, respectively.

The inter-occasion variability (IOV) was modeled on furmonertinib clearance to identify the nonstationary PK according to the following equation (Eqs. 8 and 9) [23]:

$$\kappa_{ij} = \kappa_0 \cdot (1 - OCC) + \kappa_1 \cdot OCC \quad (8)$$

$$CL_{ij}/F = CL_{TV}/F \cdot \exp\left[\kappa_{ij} + \eta_{i(CL/F)}\right] \quad (9)$$

where κ_{ij} is the IOV on the furmonertinib clearance, normally distributed with a mean of 0 and a variance of $\omega^2_{(IOV)}$. OCC is the occasion number, which equals 0 for the occasion after the single-dose treatment or the first dosing and 1 for the occasion after multiple-dose treatment. CL_{ij}/F is the predicted furmonertinib clearance for individual i on occasion j; CL_{TV}/F is the typical value for furmonertinib clearance. $\eta_{i(CL/F)}$ is an inter-individual variability, normally distributed with a mean of 0 and a variance of $\omega^2_{(CL/F)}$.

Then, a mechanistic indirect response (IDR) model III replaced the IOV to describe the nonstationary PK due to the autoinduction effect [24–31]. Furmonertinib plasma concentrations drive the enzyme amount increase, which in turn affects the clearance of the furmonertinib. The apparent clearance of furmonertinib (CL/F) was assumed to be proportional to the enzyme amount, which is expressed as the following equation (Eq. 10):

$$CL/F = CL_{base}/F \cdot A_{ENZ} \quad (10)$$

where CL_{base}/F represents baseline clearance and A_{ENZ} represents the fold change of the enzyme amount with an initial condition $A_{ENZ(0)} = 1$. The rate of change of the enzyme amount was described as the follows (Eq. 11):

$$\frac{dA_{ENZ}}{dt} = k_{ENZ} \cdot \left(1 + S \cdot \frac{A_4}{V_c}\right) - k_{ENZ} \cdot A_{ENZ} \quad (11)$$

where the parameter k_{ENZ} represents the first-order rate constant for enzyme pool degradation. The zero-order production rate of the enzyme was set to [$k_{ENZ} \cdot A_{ENZ(0)}$]. S is the slope parameter describing the relationship between drug concentration and the enzyme formation rate.

Stochastic model building. The inter-individual variability (IIV) for structural parameters was modeled using an exponential error model as follows (Eq. 12):

$$P_i = P_{TV} \cdot \exp(\eta_i) \quad (12)$$

where P_i represents the predicted value of the parameter for individual i, P_{TV} represents the typical value of the parameter, and η_i represents normally distributed random variable with a mean of 0 and variance of ω^2.

The residual variability in furmonertinib and AST5902 was added separately. Different residual error model was explored, including an additive error model with log-transformed data and a combined error (proportional plus additive) model with the untransformed data [32]. Eventually, an additive model of residual error was applied to log-transformed data and described as Eq. 13 [33]:

$$\ln Y_{ij} = \ln C_{ij} + \varepsilon_{ij} \quad (13)$$

where Y_{ij} represents the observed PK value of individual i at time t_j, C_{ij} represents the individual prediction, and ε_{ij} is a zero-mean normally distributed random variable with a variance of δ^2.

Covariate model building. The base model with autoinduction (Fig. 1) was used as a starting point for covariate modeling. The evaluated covariates included age, gender, body weight, height, BMI, dose level, food status, hepatic dysfunction, alanine transaminase (ALT), aspartate aminotransferase (AST), alkaline phosphatase (ALP), total bilirubin (TBIL), creatinine clearance (CrCl), population (NSCLC patients and healthy volunteer). Table 1 shows the summary of subjects' characteristics at baseline.

Covariate relationships were included multiplicatively as power models centered at the median values for continuous covariates or as conditional effects relative to the most common category for categorical covariates. The equations are shown below (Eqs. 14 and 15):

$$P_i = P_{TV} \cdot \left(\frac{X_{ij}}{M(X_j)}\right)_i^{\theta} \quad (14)$$

$$P_i = P_{TV} \cdot (1 + \theta_i)^{X_{ij}} \quad (15)$$

where X_{ij} the covariate of patient i for parameter P, θ_i a coefficient that reflects the covariate's effect on the parameter, and $M(X_j)$ the median of covariate X_j for the population. The food effect was included in the base model as a categorical covariate according to the results of the noncompartmental analysis (NCA) of the food effect study [20]. Its effect on absolute oral bioavailability (F) of furmonertinib and the fraction of conversion to AST5902 (Fm) was evaluated.

To facilitate the process of covariates search, the generalized additive model (GAM) analysis was used to screen the covariates [34]. Then, covariates selected by the GAM procedure were screened by stepwise forward addition followed by backward elimination

Table 1. Demographics and covariates for subjects included in the analysis.

Number of patients by study and dose						
Study	Dose (mg), number of subjects (%)					Total number of subjects (%)
	20 ($n = 2$)	40 ($n = 3$)	80 ($n = 27$)	160 ($n = 11$)	240 ($n = 11$)	
Study 001 (dose escalation)	2 (100)	3 (100)	3 (11.1)	3 (27.3)	3 (27.3)	14 (25.9)
Study 002 (dose expansion)	0 (0.0)	0 (0.0)	8 (29.6)	8 (72.7)	8 (72.7)	24 (44.4)
Study 004 (food effect study)	0 (0.0)	0 (0.0)	16 (59.3)	0 (0.0)	0 (0.0)	16 (29.6)

Baseline demographic data Continuous variables (units)	*n*	Mean	SD	Median	Minimum	Maximum
ALT (U/L)	54	21.3	11.4	19.2	7.1	67
AST (U/L)	54	22	9.2	20	9.5	54
ALP (U/L)	54	88.1	44.3	77.2	49.8	343
TBIL (μmol/L)	54	11.9	4.6	11.4	5	23.6
CrCl (mL/min)	54	101.7	25.9	98.2	62.4	174.2
Age (year)	54	48	13.9	51.5	21	68
Body weight (kg)	54	66.5	10.4	65	48	111
BMI (kg/m^2)	54	24	3	23.9	19.4	37.1
Height (cm)	54	166.1	7.8	167	147	180

Baseline demographic data Categorical variables	Category	*n*	(%)
Sex	Female	23	42.6
	Male	31	57.4
Dose level	20 mg	2	3.7
	40 mg	3	5.6
	80 mg	27	50
	160 mg	11	20.4
	240 mg	11	20.4
Hepatic dysfunction	Normal	48	88.9
	Mild dysfunction	6	11.1
Population	Heathy volunteer	16	29.6
	NSCLC patients	38	71.4
Food status[a]	Fasting	54	85.2
	Fed	16	14.8

ALT alanine transaminase, *AST* aspartate aminotransferase, *n* number of patients, *ALP* alkaline phosphatase, *TBIL* total bilirubin, *CrCl* creatinine clearance, *BMI* body mass index, *SD* standard deviation.
[a]A total of 16 subjects participated in both fed and fasted groups (crossover study) and therefore the total number of subjects exceeds 54.

method using the stepwise covariate modeling (SCM) tool in Perl Speaks-NONMEM (PsN) [35]. Significance levels of 0.05 and 0.001 were used for the forward addition and the backward elimination.

Model evaluation. Model selection and evaluation were based on the objective function value (OFV), visual inspection of graphical diagnostics and parameter precision.

The diagnostic plots included: observed concentration vs. population predicted concentration and individual predicted concentration, conditional weighted residual (CWRES) vs. population predicted concentration and CWRES vs. time. The final model was also evaluated using prediction-corrected visual predictive checks (pcVPC) [36]. Five hundred data sets were simulated by NONMEM, using the parameters estimated in the final model. A bootstrap with 500 replicates was performed in PsN on the final model to generate non-parametric 95% confidence intervals (CIs) for all parameters [37].

Model-based simulation. The PK and the time-dependent clearance were simulated to evaluate the influence of autoinduction on the nonstationary PK. The clinical trial simulation was performed using the estimated parameters from the final model. All the simulation follows the protocol of once-daily furmonertinib treatment for 21 days (1 cycle). The relative increase in furmonertinib clearance was calculated by $[(CL/F)/(CL_{base}/F)]$ according to Eqs. 10 and 11. The PK profiles of furmonertinib and AST5902 were simulated. Since both furmonertinib and AST5902 are active components, the total concentration (nmol/mL) of these two analytes was calculated and served as the concentration of the total active compounds.

Software. Population PK and simulations were performed using nonlinear mixed-effects modeling methods by NONMEM (version 7.3, ICON plc, Hanover, MD, USA), compiled with GFortran FORTRAN Compiler version 4.7.3 (Gnu Compiler Collection [GCC])

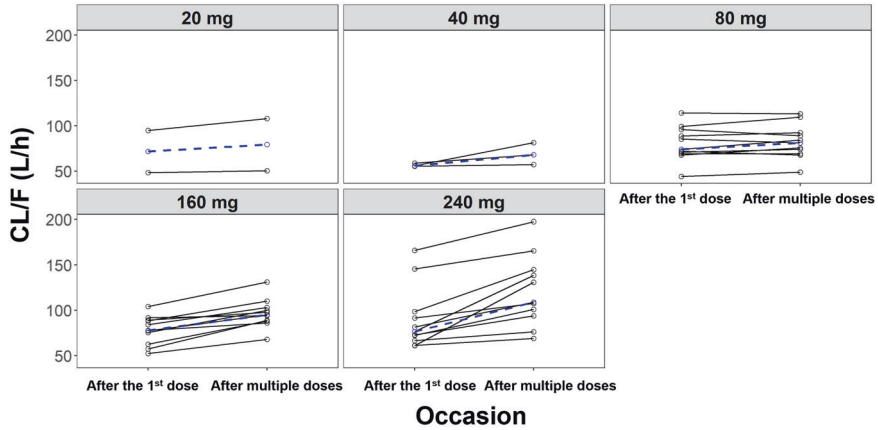

Fig. 2 Estimated furmonertinib apparent clearance on the occasions after the first administration (or the single-dose treatment, left) and multiple-dose administration (right). Blue color circle represents the median. The increase is significant in the dose group 160 and 240 mg ($P < 0.05$, paired t test).

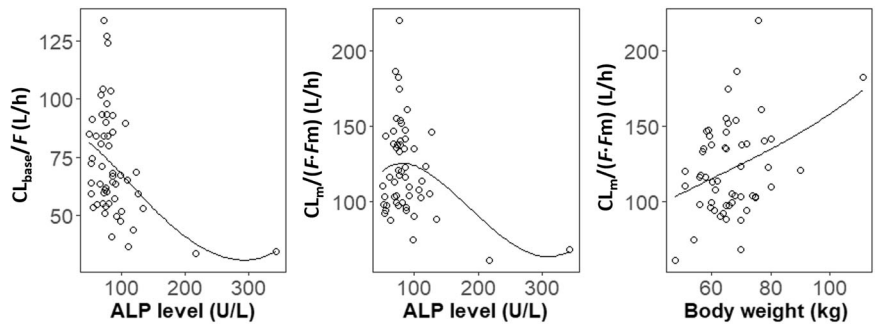

Fig. 3 Estimated apparent clearance versus the covariates. Individual baseline clearance of furmonertinib and AST5902 were plotted versus the ALP level and body weight, respectively.

in a Windows 10 operating system. For population PK analysis, a first-order conditional estimation with the interaction method was used. The use of NONMEM was facilitated with PsN (version 4.9.0, https://uupharmacometrics.github.io/PsN/). Diagnostic graphics, post-processing of the data and NONMEM outputs were performed using the R (version 3.6.1, the R Project for Statistical Computing, https://www.r-project.org/) [38].

RESULTS

Pharmacokinetic database description

In total, 1450 and 1463 plasma concentrations of furmonertinib and AST5902, respectively, collected from 38 NSCLC patients and 16 healthy subjects, were included in the analysis. Among the 38 patients and 16 healthy subjects, 23 (42.6%) were women and 31 (57.4%) were men, with a mean age of 52 years (range: 21–68 years). The detailed demographic characteristics were shown in Table 1.

Structural model identification

To capture the peak concentration of furmonertinib, the transit compartment models were used to describe the absorption of furmonertinib. With two transit compartments in the model structures, the goodness of model fitting was significantly improved in comparison with the model with one absorption compartment. More transit compartments in the model were also tested while did not further improve the model fittings.

To describe the nonstationary PK due to the autoinduction, IOV was modeled on furmonertinib clearance, which significantly reduced the OFV by 653.4 from −2353.7 to −3007.1 (corresponding to $P < 0.001$, and the parameter estimates of the IOV model were not shown). Fig. 2 shows that the clearance increased after multiple-dose treatment, and such increase appeared to correlate with dose levels, indicating the presence of self-induction on drug elimination. Then, the mechanistic IDR model III was incorporated to describe the nonstationary PK due to the autoinduction of furmonertinib metabolism. The model with the IDR model III led to a decrease in OFV by 785.9 from −2353.7 to −3139.6 (corresponding to $P < 0.001$).

Covariate model

The GAM analysis identified the following covariate effects: population, ALP and CrCL on CL/F; TBIL, ALP and body weight on V_c/F; ALT, height, body weight and BMI on k_a; gender, ALP, TBIL and body weight on $CL_m/(F \cdot Fm)$; ALP and TBIL on $V_{cm}/(F \cdot Fm)$. These covariates were further screened using the SCM, where ALP and body weight were identified as significant covariates. The relationships between covariates and clearance were presented in Fig. 3, where the baseline clearance vs. ALP level and body weight were plotted, respectively. It appeared that both the clearance of furmonertinib and AST5902 decreased with the increasing ALP level. Thus, the covariate impacts including food intake, ALP and body weight were incorporated into the final model.

Final model

The parameter estimates of the final model were provided in Table 2. All parameters were estimated with adequate precision, as shown by the relative standard errors being within 40%. Shrinkage of IIV on CL/F, V_c/F, k_a, $CL_m/(F \cdot Fm)$ and $V_{cm}/(F \cdot Fm)$ were all small (≤15%). The results of the bootstrap analysis were also presented in Table 2. As shown, the parameters were

Table 2. Final model parameter estimates.

Parameters (units)	Estimate	%RSE	Bootstrap estimate		
			Median	2.5% CI	97.5% CI
CL_{base}/F (L/h)	70.5	6.41	70.5	61.3	79.4
V_c/F (L)	2897	6.35	2837	2344	3216
k_a (1/h)	1.34	5.63	1.32	1.14	1.48
Q/F (L/h)	12.4	34.2	12.6	9.42	53.0
V_p/F (L)	1470	26.7	1499	1113	2561
k_{ENZ} (1/h)	0.00304	6.56	0.00311	0.000952	0.00560
S	0.0111	18.1	0.0112	0.00710	0.0225
$CL_m/(F \cdot Fm)$ (L/h)	119	3.56	119	111	128
$V_{cm}/(F \cdot Fm)$ (L)	291	9.27	286	215	341
k_{67} (1/h)	0.952	17.5	0.972	0.743	1.67
k_{76} (1/h)	0.0542	9.20	0.0540	0.0471	0.0711
$\theta_{CLbase/F,\ ALP}$	−0.505	17.5	−0.501	−0.679	−0.235
$\theta_{CLm/(F\cdot Fm),\ ALP}$	−0.278	32.7	−0.258	−0.430	0.0667
$\theta_{CLm/(F\cdot Fm),\ body\ weight}$	0.622	27.8	0.629	0.144	0.956
$\theta_{F,\ food}$	0.224	38.3	0.225	0.0500	0.405
$\theta_{Fm,\ food}$	−0.335	7.87	−0.332	−0.382	−0.272
$\omega^2_{CL/F}$	0.0780 (3.47)	22.2	0.0756	0.0444	0.116
$\omega^2_{Vc/F}$	0.144 (3.39)	27.1	0.142	0.0740	0.242
ω^2_{ka}	0.161 (1.11)	22.8	0.156	0.0995	0.230
$\omega^2_{CLm/(F\cdot Fm)}$	0.0485 (3.25)	19.6	0.0444	0.0284	0.0661
$\omega^2_{Vcm/(F\cdot Fm)}$	0.0970 (11.4)	29.6	0.0934	0.0463	0.163
$\delta_{ADD\ ERR\ furmonertinib}$ (CV%)	33.6 (4.02)	8.05	33.0	28.4	39.3
$\delta_{ADD\ ERR\ AST5902}$ (CV%)	27.5 (4.39)	8.54	27.1	22.8	32.3

CL_{base}/F, apparent clearance of furmonertinib at baseline; V_c/F, apparent volume of distribution of the central compartment of furmonertinib; k_a, absorption rate constant; Q/F, apparent inter-compartmental clearance of furmonertinib; V_p/F, furmonertinib apparent volume of distribution of the peripheral compartment; F, the absolute oral bioavailability of furmonertinib; Fm, the fraction of conversion to AST5902; k_{ENZ}, the first-order rate constant for enzyme degradation; S, the slope parameter describing the relationship between drug concentration and the enzyme formation rate; $CL_m/(F \cdot Fm)$, apparent clearance of AST5902; $V_{cm}/(F \cdot Fm)$, AST5902 apparent volume of distribution of the central compartment; k_{67} and k_{76}, distribution rate constant of AST5902; ADD ERR, additive error in logarithmic domain, expressed as coefficients of variation (CV%); RSE, relative standard error.
Note:
For interindividual variability terms ω^2 and residual variability δ^2, the respective shrinkage estimates are displayed in parentheses.
The equations that describe the relationships between covariates and the typical values of pharmacokinetic parameters were as follows:
$CL_{base\_TV} = 70.5 \cdot \left(\frac{ALP}{77.2}\right)^{-0.505}$,
$CL_{m\_TV} = 119 \cdot \left(\frac{ALP}{77.2}\right)^{-0.278} \cdot \left(\frac{WT}{65}\right)^{0.6216}$, where WT represents the body weight.
$F_{TV} = 1 \cdot (1 + 0.224)^{FOOD}$,
$F_{m\_TV} = 1 \cdot (1 - 0.335)^{FOOD}$, where FOOD is a categorical covariate of 1 for fed and 0 for fasting status.

estimated with good precision and the medians estimated by the bootstrap analysis were consistent with the original parameter estimates.

Model evaluation

The goodness-of-fit diagnostic plots of the final model were shown in Fig. 4. There was no obvious bias in the model fitting. The pcVPC results shown in Fig. 5 suggested that the model adequately described the nonstationary PK of both the parent and the metabolite. The general trend and the observed variability were well captured, after the first dose (Fig. 5a) and multiple-dose treatment (Fig. 5b).

Model-based simulation

The relative increase in furmonertinib apparent clearance (CL/*F*) was shown in Fig. 6a for dose groups from 20 to 240 mg. The model-based simulation predicted the relative increase from day 0 to day 21 for the typical subject in the dataset (fasting, weighing 65 kg and the ALP level at 77.2 U/L). The CL/*F* approached steady state on day 21. The result suggested that CL/*F* increased after once-daily treatment of furmonertinib for 21 days, ranging from 1.1 fold to 1.8 fold corresponding to the dose range of 20–240 mg.

The simulated drug concentrations of furmonertinib, AST5902 and the total active compounds were shown in Fig. 6b. The concentration of furmonertinib at steady state decreased over time, where the decrease in the high dose group was greater than that in the low dose group. However, the concentration of AST5902 (green line) and the total active compounds (blue line) was less influenced by the autoinduction effect, where only a slight decrease in the 240 mg dose group at steady state was observed.

The areas under the plasma concentration-time curve at steady states (AUC_{SS}) and PK profiles of furmonertinib, AST5902 and the

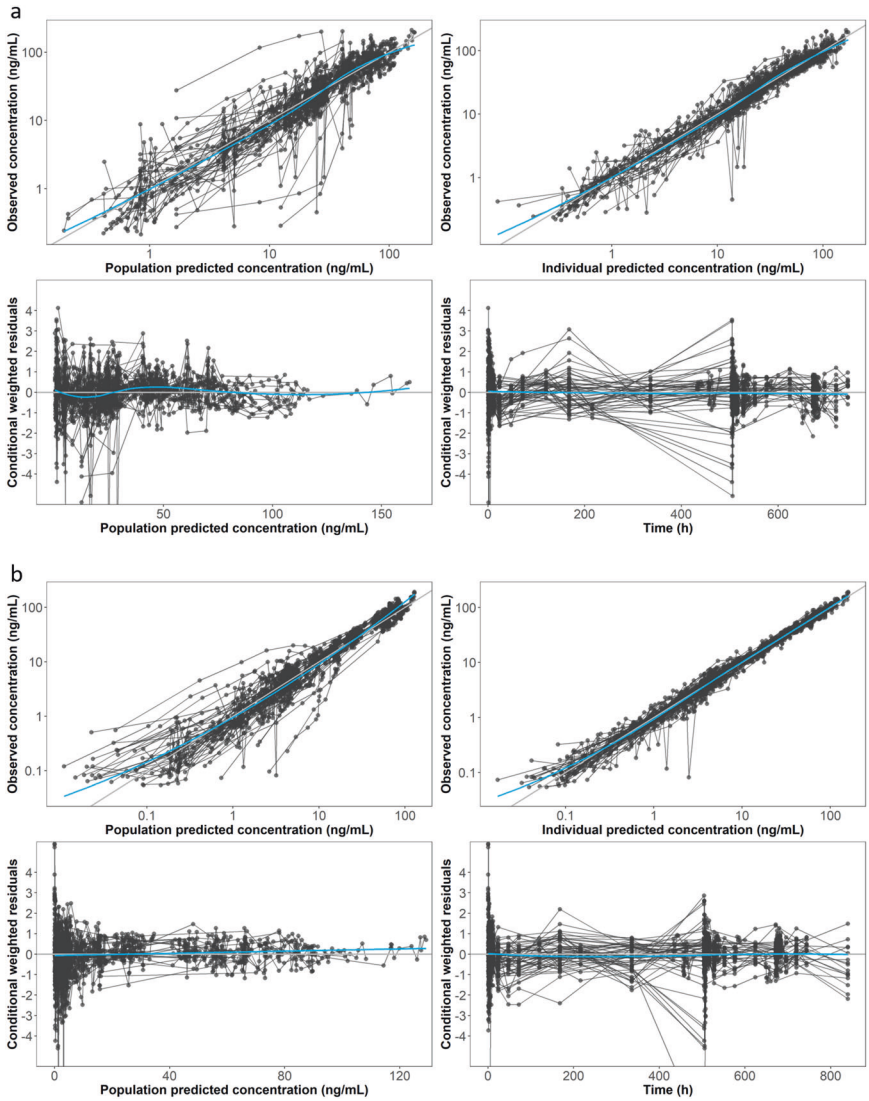

Fig. 4 General goodness-of-fit for (a) furmonertinib and (b) AST5902 of the final model. The top panels of (**a**) and (**b**) present the observed data vs. population predictions and individual predictions, respectively. The bottom panels of (**a**) and (**b**) present the CWRES vs. population predictions and time, respectively. Individual data points from the same subject are connected by black lines. The blue lines are loess smooth lines. The gray diagonal (top panels) and horizontal lines (bottom panels) are the lines of identity and zero lines, respectively.

total active compounds were simulated under different levels of the selected covariates, which were presented in Supplementary Fig. S1 and S2, respectively. The simulation results suggested that the impacts of covariates on PK of furmonertinib, AST5902 and the total active compounds were small.

DISCUSSION

Our study, for the first time, uses the PK-PD modeling to characterize the nonstationary PK of the furmonertinib and AST5902 simultaneously. Previous studies have found that furmonertinib could induce the production of the enzyme CYP3A4 and therefore increase the rate of metabolism [19]. Consistently, the apparent clearance of furmonertinib and the metabolite-parent AUC ratio increased with the dose level after multiple-dose treatment [18]. In the current study, the results from IOV modeling (as shown in Fig. 2) also showed that the furmonertinib apparent clearance after multiple-dose treatment was higher than that after single-dose treatment. Interestingly, the self-induction effect appeared to be concentration-dependent, where the increase in clearance appeared to increase with dose as shown in Fig. 2. However, three subjects showed a slight increase or even a decrease in the clearance at the 80 mg dose group. The difference in responsiveness to the autoinduction effect could be due to different hepatic function levels among those patients. The results of IOV indicated the presence of nonstationary clearance. Based on the mechanism that furmonertinib could increase the production rate of CYP3A4, the IDR III model was selected to characterize the autoinduction effect on the metabolism of furmonertinib. This model has also been widely used in other drugs with the autoinduction effect such as rifampin [27]. We initially used the E_{max} function to describe the enzyme induction effect of furmonertinib. However, the estimated maximum effect and potency parameters were extremely large, indicating over-parameterization in the model. Thus, a simpler slope parameter was used in the IDR model. The estimated k_{ENZ} value (0.00304) is reflective of the CYP3A4 half-life and agreed with previous studies [27, 39–41].

The current work supported the use of furmonertinib 80 mg dose among the evaluated dose levels. First, 80 mg furmonertinib showed similar clinical efficacy and minimum CYP3A4-inducing activity compared to higher dose levels. The previous study has

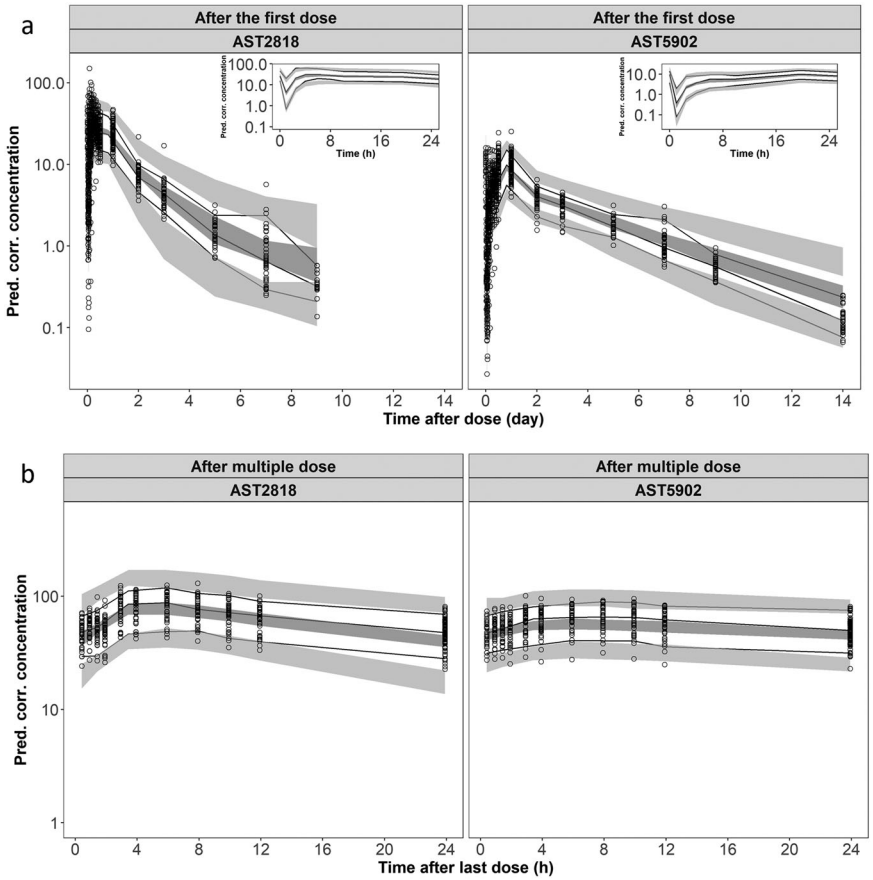

Fig. 5 Prediction-corrected visual predictive check for the concentrations of furmonertinib (AST2818) and AST5902. (a) After single-dose treatment or the first administration as well as (**b**) after multiple-dose treatment. Open circles represent the observed data. The insets show a zoom of the prediction-corrected visual predictive checks from 0 to 24 h after the first dose. The lines are the 5th, 50th, and 95th percentiles of the observed data. Shaded areas represented the 90% confidence intervals for each percentile from 500 simulations.

demonstrated that the clinical efficacies of 80, 160, and 240 mg dose are similar [18]. Also, the model-based simulation (Fig. 6a) showed that at steady-state the CYP3A4 activity, represented by furmonertinib clearance, increased about 1.3, 1.6, and 1.8 folds at 80, 160, and 240 mg dose level. This result indicated that 80 mg is less likely to cause CYP3A4-induced drug-drug interaction than 160 and 240 mg. Second, it is unlikely the slight concentration decrease in the 80 mg dose group due to autoinduction would affect drug efficacy over time, because the potency of parent and metabolite are comparable. The current study suggested that autoinduction resulted in a decrease in exposure of the parent compound but not the active metabolite. This alleviated the influence of autoinduction on the exposure of total active compounds, which is less affected by autoinduction as shown in Fig. 6b. Thus, furmonertinib 80 mg dose is preferred over 160 and 240 mg. It is worth mentioning that 80 mg is currently being evaluated in a larger phase III trial as the first-line therapy for NSCLC patients.

The impact of food intake was identified on the bioavailability of furmonertinib and the fraction of conversion to AST5902. Although such effect may not be clinically meaningful, its influence could be complex since the AUC of furmonertinib increased by 32% whereas that of active metabolite AST5902 slightly decreased (8%) [20]. For furmonertinib, the NCA results showed that its terminal slope of the PK profile did not change after food intake, suggesting that food did not affect its clearance. Also, the result of the mass-balance study [42] suggested that furmonertinib was absorbed thoroughly in vivo, indicating that the food effect could not further increase its absorption extent. Thus, the effect of food intake is more likely to increase the bioavailability of furmonertinib by increasing the splanchnic blood flow. An increase in the splanchnic blood flow could reduce the first-pass metabolism of furmonertinib, a phenomenon that has been reported in other drugs [43–46]. As for the active metabolite AST5902, under the influence of food intake, it was less produced by the first-pass metabolism whereas more via the systematic circulation of furmonertinib. The counteracting effect of the above two processes slightly reduced the exposure of AST5902. The result of the food effect implies an alternative model structure, where the AST5902 was produced by the first-pass metabolism in addition to those from the parent compound in systematic circulation [47]. However, such a model is not supported by current data. Without the intravenous PK data of both furmonertinib and metabolite, the fractions of metabolite formed via first-pass and system circulation cannot be separately identified.

In the covariate analysis, the effect of the ALP level on the PK was quantified. ALP was negatively correlated with the clearance of furmonertinib and AST5902 (Fig. 3). ALP has been identified as a significant covariate for other hepatic-elimination drugs [48]. Although the result is consistent with the mechanism that the furmonertinib is mainly eliminated by the liver, given the small number of patients in the study, more data are needed to confirm the impact of ALP on PK. Also, we found these relationships might be caused by two patients, whose ALP levels were abnormal and much higher than others (Supplementary Fig. S1). After the removal of two patients, ALP was not a significant covariate on the clearance

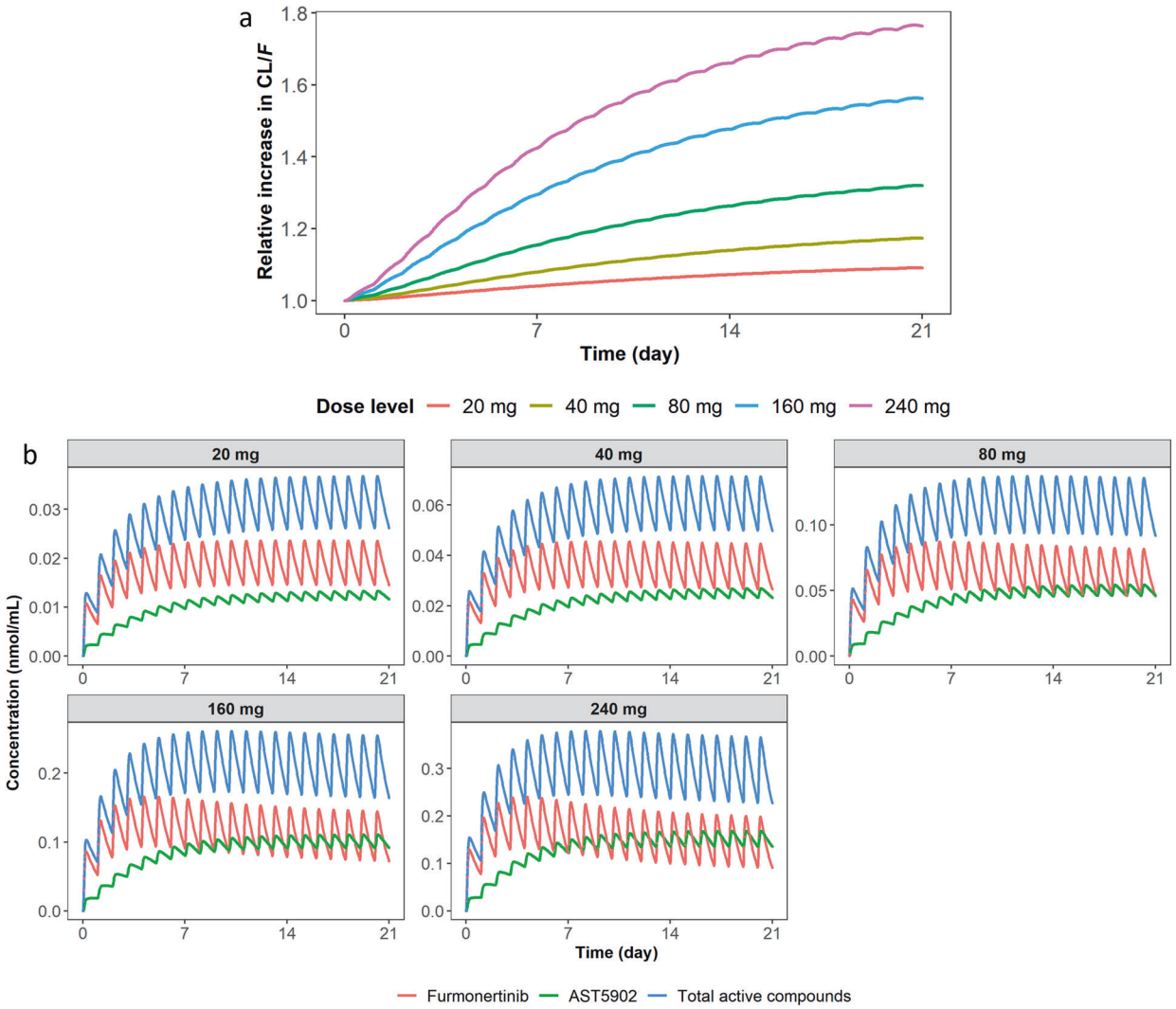

Fig. 6 Model-based simulation for the furmonertinib clearance and drug concentration. Model-based simulation of (**a**) the relative increase in furmonertinib apparent clearance (CL/*F*) and (**b**) the drug concentration of typical subjects who received once-daily furmonertinib oral administration for 21 days (one cycle).

of furmonertinib and AST5902 anymore ($P = 0.03$ vs. $P = 0.61$).

In conclusion, we have conducted population PK analysis of furmonertinib and AST5902 based on the clinical data obtained from three clinical trials, including two conducted in patients and one in healthy volunteers. A joint population PK model of furmonertinib and its metabolite AST5902 was developed, which adequately described the nonstationary PK of furmonertinib and AST5902 due to the autoinduction effect on metabolism. Based on the covariate analysis, body weight, food intake and ALP levels were identified as significant covariates. However, their influences on PK were not likely to be clinically meaningful. The current work supported the use of a once-daily furmonertinib dose of 80 mg based on its similar efficacy and minimum CYP3A4-inducing activity in comparison to the higher doses. The developed population PK model can be further used in the exposure-response analysis of furmonertinib.

ACKNOWLEDGEMENTS

We thank the investigators and patients from the studies provided data that informed the development of this model. This work was supported by the National Natural Science Foundation of China (No. 81521005) and the start-up grant from School of Pharmacy, the Chinese University of Hong Kong.

AUTHOR CONTRIBUTIONS

Conception and design of the work: XYY and Yi-fan Zhang. Modeling and simulation: HXZ and XYY. Analysis and interpretation of the data: HXZ, Yu-feng Zhang, DFZ, QYZ, YJ, FL, ZZ, Yi-fan Zhang and XYY. Drafting and revising the paper: HXZ, Yi-fan Zhang and XYY. Final approval of the paper: all authors.

ADDITIONAL INFORMATION

Supplementary information The online version contains supplementary material available at https://doi.org/10.1038/s41401-021-00798-y.

Competing interests: YJ, FL, and QYZ are employees of Shanghai Allist Pharmaceuticals Co., Ltd. The remaining authors declared no conflicts of interest.

REFERENCES

1. Dancey J, Shepherd FA, Gralla RJ, Kim YS. Quality of life assessment of second-line docetaxel versus best supportive care in patients with non-small-cell lung cancer previously treated with platinum-based chemotherapy: results of a prospective, randomized phase III trial. Lung Cancer. 2004;43:183–94.
2. Jemal A, Bray F, Center MM, Ferlay J, Ward E, Forman D. Global cancer statistics. CA: Cancer J Clinicians. 2011;61:69–90.
3. Lynch TJ, Bell DW, Sordella R, Gurubhagavatula S, Okimoto RA, Brannigan BW, et al. Activating mutations in the epidermal growth factor receptor underlying responsiveness of non–small-cell lung cancer to gefitinib. N Engl J Med. 2004;350:2129–39.

4. Prabhakar CN. Epidermal growth factor receptor in non-small cell lung cancer. Transl Lung Cancer Res. 2015;4:110.
5. Tan DS, Yom SS, Tsao MS, Pass HI, Kelly K, Peled N, et al. The international association for the study of lung cancer consensus statement on optimizing management of EGFR mutation–positive non–small cell lung cancer: status in 2016. J Thorac Oncol. 2016;11:946–63.
6. Reck M, Popat S, Reinmuth N, De Ruysscher D, Kerr K, Peters S. Metastatic non-small-cell lung cancer (NSCLC): ESMO Clinical Practice Guidelines for diagnosis, treatment and follow-up. Ann Oncol. 2014;25:iii27–39.
7. Shi Y, Zhang L, Liu X, Zhou C, Zhang S, Wang D, et al. Icotinib versus gefitinib in previously treated advanced non-small-cell lung cancer (ICOGEN): a randomised, double-blind phase 3 non-inferiority trial. Lancet Oncol. 2013;14:953–61.
8. Shi YK, Wang L, Han BE, Li W, Yu P, Liu Y, et al. First-line icotinib versus cisplatin/pemetrexed plus pemetrexed maintenance therapy for patients with advanced EGFR mutation-positive lung adenocarcinoma (CONVINCE): a phase 3, open-label, randomized study. Ann Oncol. 2017;28:2443–50.
9. Hanna N, Johnson D, Temin S, Baker S Jr, Brahmer J, Ellis PM, et al. Systemic therapy for stage IV non–small-cell lung cancer: American Society of Clinical Oncology clinical practice guideline update. J Clin Oncol. 2017;33:3488.
10. Maemondo M, Inoue A, Kobayashi K, Sugawara S, Oizumi S, Isobe H, et al. Gefitinib or chemotherapy for non–small-cell lung cancer with mutated EGFR. N Engl J Med. 2010;362:2380–8.
11. Mitsudomi T, Morita S, Yatabe Y, Negoro S, Okamoto I, Tsurutani J, et al. Gefitinib versus cisplatin plus docetaxel in patients with non-small-cell lung cancer harbouring mutations of the epidermal growth factor receptor (WJTOG3405): an open label, randomised phase 3 trial. Lancet Oncol. 2010;11:121–8.
12. Rosell R, Carcereny E, Gervais R, Vergnenegre A, Massuti B, Felip E, et al. Erlotinib versus standard chemotherapy as first-line treatment for European patients with advanced EGFR mutation-positive non-small-cell lung cancer (EURTAC): a multicentre, open-label, randomised phase 3 trial. Lancet Oncol. 2012;13:239–46.
13. Helena AY, Arcila ME, Rekhtman N, Sima CS, Zakowski MF, Pao W, et al. Analysis of tumor specimens at the time of acquired resistance to EGFR-TKI therapy in 155 patients with EGFR-mutant lung cancers. Clin Cancer Res. 2013;19:2240–7.
14. Kobayashi S, Boggon TJ, Dayaram T, Jänne PA, Kocher O, Meyerson M, et al. EGFR mutation and resistance of non–small-cell lung cancer to gefitinib. N Engl J Med. 2005;352:786–92.
15. Murtuza A, Bulbul A, Shen JP, Keshavarzian P, Woodward BD, Lopez-Diaz FJ, et al. Novel third-generation EGFR tyrosine kinase inhibitors and strategies to overcome therapeutic resistance in lung cancer. Cancer Res. 2019;79:689–98.
16. Mok TS, Wu YL, Ahn MJ, Garassino MC, Kim HR, Ramalingam SS, et al. Osimertinib or platinum–pemetrexed in EGFR T790M-positive lung cancer. N Engl J Med. 2017;376:629–40.
17. Shi Y, Hu X, Zhang S, Lv D, Wu L, Yu Q, et al. Efficacy, safety, and genetic analysis of furmonertinib (AST2818) in patients with EGFR T790M mutated non-small-cell lung cancer: a phase 2b, multicentre, single-arm, open-label study. Lancet Respiratory Med. 2021;9:829–39.
18. Shi Y, Zhang S, Hu X, Feng J, Ma Z, Zhou J, et al. Safety, clinical activity, and pharmacokinetics of alflutinib (AST2818) in patients with advanced NSCLC with EGFR T790M mutation. J Thorac Oncol. 2020;15:1015–26.
19. Liu XY, Guo ZT, Chen ZD, Zhang YF, Zhou JL, Jiang Y, et al. Alflutinib (AST2818), primarily metabolized by CYP3A4, is a potent CYP3A4 inducer. Acta Pharmacol Sin. 2020;41:1366–76.
20. Zhu S, Deng J, Tang Q, Heng J, Qu J, Chen Y, et al. A randomized, open, single-centre, crossed study of the effect of food on the pharmacokinetics of one oral dose of alflutinib mesylate tablets (AST2818) in healthy male subjects. Iran J Pharm Res. 2020;19:24–33.
21. Liu X, Li W, Zhang Y, Jiang Y, Zhao Q, Zhong D. Simultaneous determination of alflutinib and its active metabolite in human plasma using liquid chromatography-tandem mass spectrometry. J Pharm Biomed Anal. 2019;176:112735.
22. Cosson V, Jorga K, Fuseau E. Modeling of metabolite pharmacokinetics in a large pharmacokinetic data set and application. Pharmacometrics: the science of quantitative pharmacology. Wiley 2007:1107–36.
23. Karlsson M, Sheiner L. The importance of modeling interoccasion variability in population pharmacokinetic analyses. J Pharmacokinet Biopharm. 1993;21:735–50.
24. Dayneka NL, Garg V, Jusko WJ. Comparison of four basic models of indirect pharmacodynamic responses. J Pharmacokinet Biopharm. 1993;21:457–78.
25. Gordi T, Xie R, Huong NV, Huong DX, Karlsson MO, Ashton M. A semiphysiological pharmacokinetic model for artemisinin in healthy subjects incorporating autoinduction of metabolism and saturable first-pass hepatic extraction. Br J Clin Pharmacol. 2005;59:189–98.
26. Gordi T, Xie R, Jusko WJ. Semi-mechanistic pharmacokinetic/pharmacodynamic modelling of the antimalarial effect of artemisinin. Br J Clin Pharmacol. 2005;60:594–604.
27. Smythe W, Khandelwal A, Merle C, Rustomjee R, Gninafon M, Bocar Lo M, et al. A semimechanistic pharmacokinetic-enzyme turnover model for rifampin autoinduction in adult tuberculosis patients. Antimicrob Agents Chemother. 2012;56:2091–8.
28. Svensson RJ, Aarnoutse RE, Diacon AH, Dawson R, Gillespie SH, Boeree MJ, et al. A Population Pharmacokinetic Model incorporating saturable pharmacokinetics and autoinduction for high rifampicin doses. Clin Pharmacol Ther. 2018;103:674–83.
29. Chirehwa MT, Rustomjee R, Mthiyane T, Onyebujoh P, Smith P, McIlleron H, et al. Model-based evaluation of higher doses of rifampin using a semimechanistic model incorporating autoinduction and saturation of hepatic extraction. Antimicrob Agents Chemother. 2016;60:487–94.
30. Hassan M, Svensson US, Ljungman P, Björkstrand B, Olsson H, Bielenstein M, et al. A mechanism-based pharmacokinetic-enzyme model for cyclophosphamide autoinduction in breast cancer patients. Br J Clin Pharmacol. 1999;48:669.
31. Kerbusch T, Huitema A, Ouwerkerk J, Keizer H, Mathôt R, Schellens J, et al. Evaluation of the autoinduction of ifosfamide metabolism by a population pharmacokinetic approach using NONMEM. Br J Clin Pharmacol. 2000;49:555–61.
32. Girard P. Eleventh Meeting, Population Approach Group in Europe. p. 6–7.
33. Edlund H, Lee SK, Andrew MA, Slatter JG, Aksenov S, Al-Huniti N. Population pharmacokinetics of the BTK inhibitor acalabrutinib and its active metabolite in healthy volunteers and patients with B-cell malignancies. Clin Pharmacokinet. 2019;58:659–72.
34. Wählby U, Jonsson EN, Karlsson MO. Comparison of stepwise covariate model building strategies in population pharmacokinetic-pharmacodynamic analysis. Aaps Pharmsci. 2002;4:68–79.
35. Jonsson EN, Karlsson MO. Automated covariate model building within NONMEM. Pharmacol Res. 1998;15:1463–8.
36. Bergstrand M, Hooker AC, Wallin JE, Karlsson MO. Prediction-corrected visual predictive checks for diagnosing nonlinear mixed-effects models. AAPS J. 2011;13:143–51.
37. Yafune A, Ishiguro M. Bootstrap approach for constructing confidence intervals for population pharmacokinetic parameters. I: a use of bootstrap standard error. Stat Med. 1999;18:581–99.
38. Team RCR Core Team. R: A language and environment for statistical computing. Foundation for Statistical Computing 2014.
39. Warren JW Jr, Benmaman JD, Wannamaker BB, Levy RH. Kinetics of a carbamazepine-ethosuximide interaction. Clin Pharmacol Ther. 1980;28:646–51.
40. Yin OQ, Wang Y, Schran H. A mechanism-based population pharmacokinetic model for characterizing time-dependent pharmacokinetics of midostaurin and its metabolites in human subjects. Clin Pharmacokinet. 2008;47:807–16.
41. von Bahr C, Steiner E, Koike Y, Gabrielsson J. Time course of enzyme induction in humans: effect of pentobarbital on nortriptyline metabolism. Clin Pharmacol Ther. 1998;64:18–26.
42. Meng J, Zhang H, Bao J, Chen Z, Liu X, Zhang Y, et al. Metabolic disposition of the EGFR covalent inhibitor furmonertinib in humans. Acta Pharmacol Sin. 2021. https://doi.org/10.1038/s41401-021-00667-8.
43. Melander A. Influence of food on the bioavailability of drugs. Clin Pharmacokinet. 1978;3:337–51.
44. McLean AJ, McNamara PJ, DuSouich P, Gibaldi M, Lalka D. Food, splanchnic blood flow, and bioavailability of drugs subject to first-pass metabolism. Clin Pharmacol Ther. 1978;24:5–10.
45. Kochak GM. Critical analysis of hepatic clearance based on an advection mass transfer model and mass balance. J Pharm Sci. 2020;109:2059–69.
46. de Jong J, Sukbuntherng J, Skee D, Murphy J, O'Brien S, Byrd JC, et al. The effect of food on the pharmacokinetics of oral ibrutinib in healthy participants and patients with chronic lymphocytic leukemia. Cancer Chemother Pharmacol. 2015;75:907–16.
47. Bertrand J, Laffont CM, Mentré F, Chenel M, Comets E. Development of a complex parent-metabolite joint population pharmacokinetic model. AAPS J. 2011;13:390–404.
48. Minami H, Kawada K, Sasaki Y, Tahara M, Igarashi T, Itoh K, et al. Population pharmacokinetics of docetaxel in patients with hepatic dysfunction treated in an oncology practice. Cancer Sci. 2009;100:144–9.